Accepted Manuscript

Long-distance seed dispersal affects the resilience of banded vegetation patterns in semi-deserts

Jamie J.R. Bennett, Jonathan A. Sherratt

Please cite this article as: Jamie J.R. Bennett, Jonathan A. Sherratt, Long-distance seed dispersal affects the resilience of banded vegetation patterns in semi-deserts, *Journal of Theoretical Biology* (2018), doi: https://doi.org/10.1016/j.jtbi.2018.10.002

Highlights

- A model for banded vegetation patterns is analysed that includes non-local seed dispersal.

- Numerical continuation and bifurcation analysis is applied to map the stability of patterns.

- Non-local seed dispersal can increase the ecological resilience of banded patterns.

- Coping strategies for critically low levels of rainfall are oscillating band densities and non-migrating patterns.

Long-distance seed dispersal affects the resilience of banded vegetation patterns in semi-deserts☆

Jamie J.R. Bennett[1], Jonathan A. Sherratt

Department of Mathematics and Maxwell Institute for Mathematical Sciences, Heriot-Watt University, Edinburgh EH14 4AS, UK

Abstract

Landscape-scale vegetation stripes (tiger bush) observed on the gentle slopes of semi-arid regions are useful indicators of future ecosystem degradation and catastrophic shifts towards desert. Mathematical models like the Klausmeier model—a set of coupled partial differential equations describing vegetation and water densities in space and time—are central to understanding their formation and development. One assumption made for mathematical simplicity is the local dispersal of seeds via a diffusion term. In fact, a large amount of work focuses on fitting dispersal 'kernels', probability density functions for seed dispersal distance, to empirical data of different species and modes of dispersal. In this paper we address this discrepancy by analysing an extended Klausmeier model that includes long-distance seed dispersal via a non-local convolution term in place of diffusion, and assessing its effect on the resilience of striped patterns. Many authors report a slow uphill migration of stripes; but others report no detectable migration speed. We show that long-distance seed dispersal permits the formation of patterns with a very slow (possibly undetectable) migration speed, and even stationary patterns which could explain the inconsistencies in the empirical data. In general, we show that the resilience of patterns to reduced rainfall may vary significantly depending on the rate of seed dispersal and the width of the dispersal kernel, and compare a selection of ecologically relevant kernels to examine the variation in pattern resilience.

Keywords: banded vegetation, non-local, seed dispersal, desertification, resilience, self-organisation, tiger bush, reaction-diffusion-advection, periodic travelling wave

1. Introduction

1.1. Ecological background

The first scientific documentation of banded vegetation (or "tiger bush") was in Somalia in the 1950s [1]. Regular bands of vegetation alternating with near bare desert were observed to run parallel to the contours of gentle slopes ($0.2 - 2\%$ incline [2]). Over the years, it has become clear that banded vegetation is a global phenomenon with recorded observations in the African Sahel [3, 4], the Mulga Lands in East Australia [5, 6, 7], the States of Nevada [8] and Texas [9] in the United States, the Sonoran Desert in northern Mexico/southern United States [10], the Negev in Israel [11] and Ladakh in India [12]. The common theme is a semi-arid climate where the heat and lack of rainfall creates a hostile environment in which plants must compete for water—the limiting factor for vegetation growth. When rainfall does occur, it is often torrential and runs off the bare, crusted ground downhill towards the vegetation where roots allow for increased infiltration; promoting plant growth on the uphill edge and plant loss on the downhill edge. Sometimes called the "water redistribution hypothesis" [13], the process generates stripes (typically 20-200m in width [2]) that slowly migrate uphill at reported speeds in the region of 0.2m to 1.5m per year [14, 15, 16, 2].

Banded vegetation patterns are not just a fascinating example of landscape scale self-organisation; they are an important stage in the process of desertification in response to climate change. Evidence of expanding deserts is clear, with recent work [17] showing a substantial advancement of the Sahara desert over the last century. A common school of thought is that desertification is a transition of uniform steady states; from a vegetation rich state to a barren 'zero' steady state where vegetation is scarce. In this regard, mathematical modelling has been instrumental in identifying the intermediate (heterogeneous) states in between, and for devising early warning signals that aid the management of expanding deserts [18, 19, 20]. For instance, the gradual changes in spatial characteristics of bands can indicate an imminent regime shift [21]—reduced rainfall leads to narrowing bands and widening gaps between them. Certain changes could be an indication that the current configuration is reaching a tipping
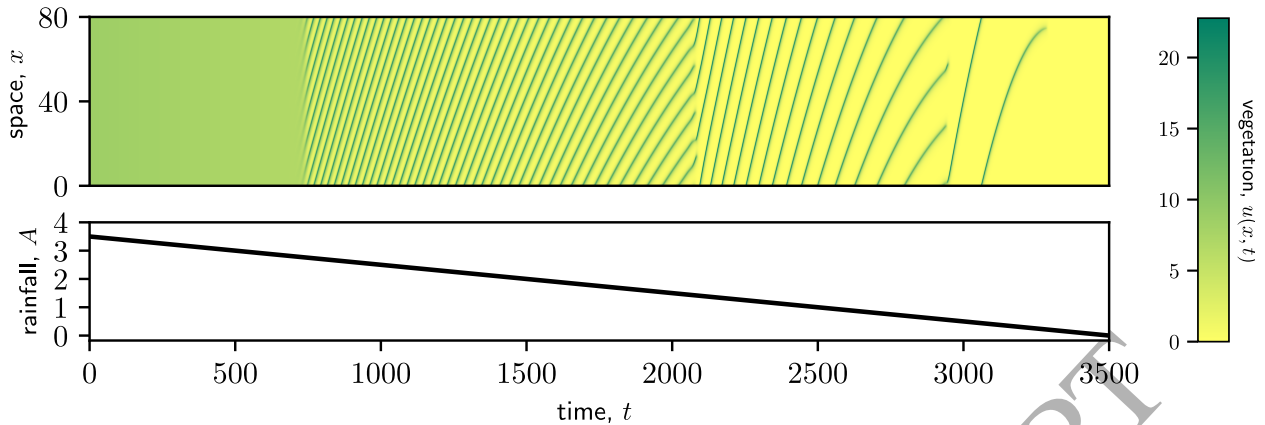
Figure 1: An illustration of desertification in one space dimension. For simplicity, rainfall slowly decreases at a constant rate from $A = 3.5$ to $A = 0$. At the beginning of the simulation uniform vegetation is sustainable but as rainfall is decreased, a pattern emerges at around $t = 750$. Patterns then transition with longer wavelengths observed for lower levels of rainfall. A single island of vegetation develops near $t = 3000$ which vanishes suddenly into bare desert. Notice the slowing down of uphill migration before each pattern transition—a useful warning signal of an imminent regime shift in practice. The numerical simulation approximates the non-local Klausmeier model (4) when seeds disperse according to the Laplace kernel (6) with $a = 1$. Other model parameters are fixed: $B = 0.45$, $v = 182.5$, $d = 1$.

point, whereupon a switch to a new pattern of vegetation will begin; a significant increase in rainfall is then needed to restore the previous state. This process can repeat itself for a predictable sequence of patterns ending with a bare desert state, as we demonstrate in Figure 1 in one space dimension. Recent work has focused on the colonisation of bare desert by vegetation [22], though in this paper we assume a starting point of uniform vegetation.

Experimental work on vegetation patterns is difficult due to their large spatial scale and slow evolution which occurs over decades. Moreover, banded patterns have never been recreated under laboratory conditions. Mathematical models are an inexpensive tool for investigating the affects of environmental change, with models that focus on the water redistribution hypothesis [23, 11, 24, 25] being popular for analysis. This paper is based on the Klausmeier model [26] which when suitably non-dimensionalised is the reaction-advection-diffusion system

$$\frac{\partial u}{\partial t} = \overbrace{u^2 w}^{\text{plant growth}} - \overbrace{Bu}^{\text{plant loss}} + \overbrace{\frac{\partial^2 u}{\partial x^2}}^{\substack{\text{local} \\ \text{plant dispersal}}}, \quad (1a)$$

$$\frac{\partial w}{\partial t} = \underbrace{A}_{\text{rainfall}} - \underbrace{w}_{\text{evaporation}} - \underbrace{u^2 w}_{\substack{\text{water uptake} \\ \text{by plants}}} + \underbrace{v\frac{\partial w}{\partial x}}_{\substack{\text{water flow} \\ \text{downhill}}} + \underbrace{d\frac{\partial^2 w}{\partial x^2}}_{\substack{\text{water} \\ \text{diffusion}}}, \quad (1b)$$

where the plant density $u(x,t)$ and surface water density $w(x,t)$ are functions of space x and time t. The one-dimensional domain is perpendicular to the contours of the slope, which we assume to be of constant gradient. A large amount of empirical evidence suggests that water infiltration in semi-arid regions is positively correlated with plant coverage due to the presence of root networks. This process forms a positive feedback loop—more vegetation leads to increased infiltration of water, which stimulates further growth of vegetation. This justifies the non-linearity in (1) which is one of the main drivers for pattern formation. Of course, on its own this would lead to unbounded growth and spread of vegetation, however, surface water is limited and acts as an inhibitor over long range via advection and

diffusion terms. These actions are responsible for pattern formation in (1). The original Klausmeier model did not include water diffusion but this has now become a common addition since it allows the formation of patterns on flat ground as reported by some authors [7]. The parameters $A > 0$, $B > 0$, $v > 0$, $d > 0$ are rates that represent the extent of rainfall, plant loss due to natural death and herbivory, the gradient of the slope, and water diffusion, respectively. We refer to (1) throughout the text as the "local Klausmeier model".

1.2. Modelling non-local seed dispersal

Recent modelling studies have focused on better understanding the role of long-range dispersal in ecological pattern formation [27, 28, 29], for instance, it was recently shown that movement of mussels via a Lévy walk creates patterns that increase ecological resilience [30]. Almost all model analysis for patterned vegetation assumes local dispersal of plants via a diffusion term, which is rarely an accurate representation of a particular plant species, but a convenient mathematical simplification. Diffusion is widely believed to be inadequate for modelling plant dispersal due to frequent long range dispersal events. The distance a seed can travel from its source is influenced by external factors such as wind, as well as species specific characteristics, e.g. height of plant, seed weight—some plant species can even disperse seeds ballistically [31]. Secondary dispersal via animal or water transport can also affect the distance a seed can travel from its source [32].

This long range reproductive behaviour can be modelled using a 'dispersal kernel', which is a probability density function, $\phi(x,t)$, describing the distribution of distances travelled by seeds originating from a single parent. As before, we let $u(x,t)$ describe the plant density at location x at time t. Suppose individual plants (seeds) disperse instantaneously from their current location x to a new lo-

3

cation y at rate $C > 0$. We can describe this process via convolution of ϕ and u and formulate the non-local analogue of the classical diffusion equation:

$$\frac{\partial u}{\partial t}(x,t) = C\left(I(x,t) - u(x,t)\right), \tag{2}$$

where $I(x,t) = (\phi * u)(x,t) = \int_{-\infty}^{\infty} \phi(x-y)u(y,t)dy.$ (3)

One can derive (2) in a stochastic setting as a point jump or kangaroo process—see for example, [33]. The probability density function $\phi(x)$ has the property $\int_{-\infty}^{\infty} \phi(x)dx = 1$, and since (2) has no births or deaths, we expect the total plant population to be conserved across the domain: the second term in (2), $-Cu$, ensures $\frac{\partial}{\partial t}\int_{-\infty}^{\infty} u(x,t)\mathrm{d}x = 0$.

This gives us a non-local description of seed dispersal and so we now define the non-local Klausmeier model,

$$\frac{\partial u}{\partial t} = \overbrace{u^2 w}^{\text{plant growth}} - \overbrace{Bu}^{\text{plant loss}} + \overbrace{C(I-u)}^{\substack{\text{non-local} \\ \text{plant dispersal}}}, \tag{4a}$$

$$\frac{\partial w}{\partial t} = \underbrace{A}_{\text{rainfall}} - \underbrace{w}_{\text{evaporation}} - \underbrace{u^2 w}_{\substack{\text{water uptake} \\ \text{by plants}}} + \underbrace{v\frac{\partial w}{\partial x}}_{\substack{\text{water flow} \\ \text{downhill}}} + \underbrace{d\frac{\partial^2 w}{\partial x^2}}_{\substack{\text{water} \\ \text{diffusion}}}, \tag{4b}$$

by replacing the diffusion term in (1) with the non-local convolution term in (2). In this paper, our primary concern is the rainfall parameter, A, and so we fix $B = 0.45$, $v = 182.5$, $d = 1$ throughout the paper. Also of interest is the effect that seed dispersal has on pattern formation via variation of parameters a and C. We shall see that varying C appropriately with a allows the local and non-local Klausmeier models to be easily compared for special dispersal kernels. All parameter choices are in accordance with recent work [28] deriving analytic results on pattern existence in (4).

1.3. Pattern existence

We begin by examining the stability of the homogeneous steady states—those relevant for pattern formation are linearly stable to homogeneous perturbations and unstable to heterogeneous perturbations. The non-local Klausmeier model has either one or three homogeneous steady states: a bare desert state $(0, A)$ that is always linearly stable, and two coexistence steady states

$$(u_\pm, w_\pm) = \left(\frac{A \pm \sqrt{A^2 - 4B^2}}{2B}, \frac{A \mp \sqrt{A^2 - 4B^2}}{2}\right), \tag{5}$$

that exist only when $A \geq 2B$, i.e. when the rate of rainfall is sufficient to support the ecosystem. The steady state (u_-, w_-) is always unstable, while (u_+, w_+) is locally stable to homogeneous perturbations when $B < 2$. It is therefore the (in)stability of (u_+, w_+) that is of primary interest when studying pattern formation. Note that when $B > 2$, oscillatory dynamics can occur that are not observed in practice. Here, we assume $B < 2$ to analyse Turing-like patterns that are generated in response to (u_+, w_+)

becoming unstable. Specifically, pattern solutions of (4) (and (1)) develop in response to a "Turing-Hopf" bifurcation which, unlike the classic (stationary) Turing pattern, gives rise to a constant uphill migration of the pattern—a standard feature of models with directed transport.

To investigate how rainfall influences pattern formation, we take A to be a control parameter. Suppose the rainfall is sufficient to support a uniform covering of vegetation, i.e. (u_+, w_+) is stable to heterogeneous (and homogeneous) perturbations. Suppose also that climate change causes the rainfall in our model ecosystem to gradually decline. At some critical value of $A \geq 2B$, (u_+, w_+) becomes unstable to heterogeneous perturbations despite remaining stable to homogeneous perturbations. This critical rainfall rate, A_{TH}, is a Turing-Hopf bifurcation. In general for both (1) and (4) an analytic expression for A_{TH} in terms of model parameter alone cannot be derived, however, leading order expressions for large v (steep slopes) have been calculated. In the local model a result of this type can be found for $d = 0$ in [34], while recent work yields an expression for the non-local Klausmeier model for the case when ϕ is the Laplacian kernel [28]. These calculations rely on expansions of the 'dispersion relation' which associates spatially heterogeneous perturbations with their respective growth rates. The difficulty with the non-local case is that one obtains the Fourier transform of the dispersion kernel within the dispersion relation. The Fourier transform of the Laplace kernel is simple enough algebraically to permit further analysis, but this is not the case for the vast majority of ecologically relevant kernels.

The existence of patterns for $A < 2B$, i.e. when a uniform covering of vegetation is no longer sustainable, reflects the increased resilience of pattern forming vegetation. The minimum rainfall supporting patterned vegetation, A_{min}, cannot be calculated analytically, though a leading order expression for large v and $d = 0$ in the local model can been found in [35]. In this paper we calculate the boundaries of pattern existence numerically, and our results for A_{TH} are in agreement with the leading order expressions in [28].

1.4. Aims

In this paper we are concerned with existing striped patterns and their resilience to ecological change. Previous work with respect to pattern stability and resilience has focused on the local Klausmeier model and is well understood thanks to the numerical continuation methods developed in [36]. The basis of this method is to be able to reduce the model to a set of ordinary differential equations. In general, the complication when considering non-local seed dispersal is that the convolution integral makes (4) non-reducible in this sense, and obtaining results similar to the local case for general ϕ is still an open problem. That being said, kernels with certain properties are reducible and this is the focus of Section 2, where we analyse (4) when ϕ is the Laplace kernel—an ecologically relevant kernel [37, 31]. In this special case we can gain

insight into the effects that long range seed dispersal has on the resilience of patterns.

Although rigorous results for general ϕ are beyond the scope of this paper, we attempt to compare kernels in Section 3 by discretising the non-local Klausmeier model in space. The size of the resulting system of ordinary differential equations would be too large for accurate results to be computationally feasible using similar methods to those employed in Section 2. To facilitate computation, we use a fixed coarse spatial grid for our discretisation, and analyse the resulting system for various ϕ. The assumption is that the error associated with the discretisation should be roughly the same regardless of the specified kernel, making the qualitative results comparable. We will show that our results in this section are surprisingly accurate by running the computations for the known diffusion and Laplace cases.

2. Laplace kernel

2.1. Local equations for a non-local model

There are numerous studies on the analysis of pattern solutions of the local Klausmeier model, with the method of Rademacher [36] being a powerful tool to test pattern stability. A prerequisite for this method is a local PDE model which one can reduce to a set of first order ordinary differential equations. This means that analysis of the non-local Klausmeier model calls for a different approach when considering the convolution integral in its full generality. That being said, dispersal kernels with special properties allow the non-local problem (4) to be recast as a set of local equations, facilitating the use of existing methods.

The Laplace kernel, often presented as the equivalent negative exponential kernel in the ecology literature [37], is given by

$$\phi(x) = \frac{a}{2}\exp\left(-a|x|\right), \quad a > 0, \tag{6}$$

and has frequently been used to fit empirical data on seed dispersal [31]. For this choice of kernel we can reduce (4) to a local PDE model, following work by other authors [38, 39, 40, 41]. First, note that the Fourier transform of ϕ is $\hat{\phi}(\xi) = a^2/(a^2 + \xi^2)$. Taking the Fourier transform of the second derivative of $I(x,t)$ and then rearranging gives,

$$\widehat{\frac{\partial^2 I}{\partial x^2}}(\xi, t) = -\xi^2 \widehat{(\phi * u)}(\xi, t)$$
$$= -\frac{a^2 \xi^2}{a^2 + \xi^2}\hat{u}(\xi, t)$$
$$= a^2\left(\frac{a^2}{a^2 + \xi^2} - 1\right)\hat{u}(\xi, t)$$

and now taking the inverse Fourier transform of this equation yields,

$$\frac{\partial^2 I}{\partial x^2}(x, t) = a^2(I(x, t) - u(x, t)).$$

The convolution integral (3) with $\phi(x)$ given by (6) can therefore be represented instead by the addition of a third equation so that we can write (4) as the local PDE model:

$$\frac{\partial u}{\partial t} = u^2 w - Bu + C(I - u), \tag{7a}$$

$$\frac{\partial w}{\partial t} = A - w - u^2 w + v\frac{\partial w}{\partial x} + d\frac{\partial^2 w}{\partial x^2}, \tag{7b}$$

$$0 = a^2(u - I) + \frac{\partial^2 I}{\partial x^2}. \tag{7c}$$

Solutions of (7) are in direct correspondence with the solutions of (4).

In the interest of model comparison with (1), we can set $C = a^2 = 2/\sigma(a)^2$, where σ is the standard deviation of
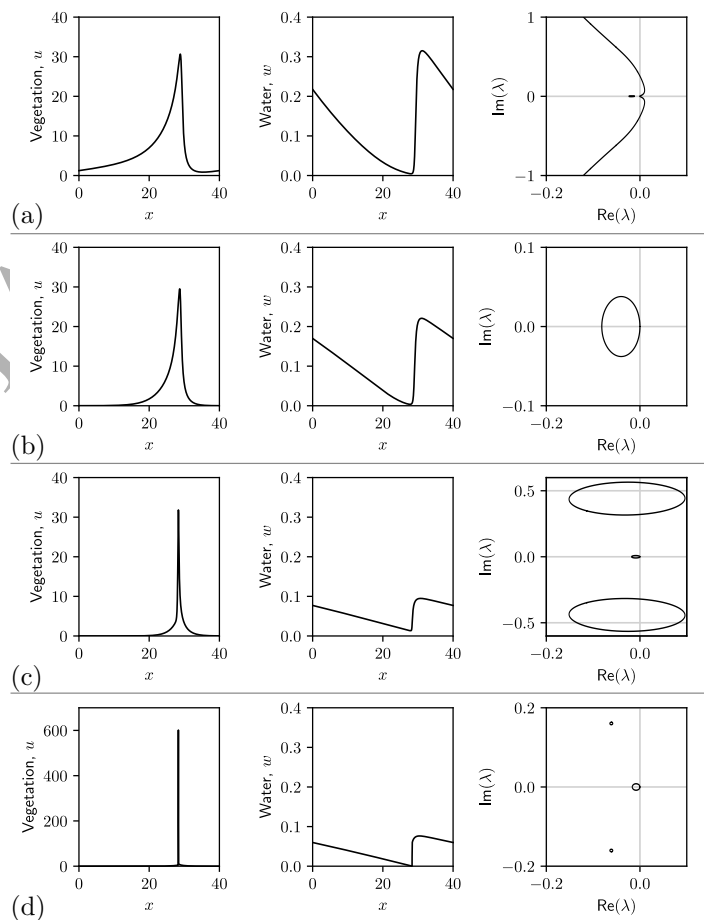

Figure 2: Travelling wave solution profiles of (8) as rainfall is decreased, along with the rightmost part of their spectra. Solutions all have a wavelength of 40 and are depicted in Figure 3(c) as green points along the constant wavelength contour. In (a) $c = 1.7$ and the pattern is unstable due to an Eckhaus instability. In (b) $c = 1$ and the pattern is stable. In (c) $c = 0.1$ and the pattern becomes unstable again but this time due to a Hopf-type instability. In (d) $c = 0.01$ and the pattern becomes stable again. Our results suggest that as c approaches its minimum value along the contour, u approaches a δ function. Other model parameters are fixed: $B = 0.45$, $v = 182.5$, $d = 1$.

5

the Laplace kernel. This ensures that in the limit $a \to \infty$, the non-local Klausmeier model with ϕ given by (6) will converge to the local Klausmeier model. This is because $C\phi$ approaches a δ function as a becomes large, i.e. seed dispersal becomes progressively more locally concentrated. This assumption requires the restriction $a > \sqrt{B}$ to ensure the existence of a maximum rainfall level for pattern formation.

2.2. Methods

The key to understanding desertification is the transition of patterns due to instability driven by low rainfall rates, and in this section we show how one can create a map of stability using numerical continuation and bifurcation analysis. This enables us to assess the differences in the critical rainfall thresholds in the presence of non-local dispersal. The study of pattern solutions of (7) is made significantly easier with a coordinate transformation to a moving frame of reference $z = x - ct$, so that travelling waves $u(x,t) = U(z)$, $w(x,t) = W(z)$, $I(x,t) = J(z)$ are solutions of

$$0 = U^2 W - BU + a^2(J - U) + cU' \qquad (8a)$$

$$0 = A - W - U^2 W + (c + v)W' + dW'' \qquad (8b)$$

$$0 = a^2(U - J) + J''. \qquad (8c)$$

Here, prime denotes differentiation with respect to z, and c is the wave speed of the pattern. Using the numerical continuation software package AUTO 07p [42] one can vary a model parameter, c say, and detect Hopf bifurcations in (8)—the birth of periodic patterns. In Figure 2 we show some solution profiles along a branch emanating from a detected Hopf bifurcations. Note that the reduction of (7) to (8) greatly simplifies analysis, but in doing so introduces an extra parameter c so that, instead of a pattern forming interval $A \in (A_{min}, A_{TH})$ described in Section 1.3, we must consider a pattern forming region in the A–c parameter plane.

Though we are able to numerically generate patterns of different wave speeds using (8), they may or may not be stable as solutions of (7). To test the stability of patterns consider the perturbed travelling waves

$$\begin{aligned} u(\xi,t) &= U(\xi) + \bar{u}(\xi,t)\exp(\lambda t), \\ w(\xi,t) &= W(\xi) + \bar{w}(\xi,t)\exp(\lambda t), \\ I(\xi,t) &= J(\xi) + \bar{I}(\xi,t)\exp(\lambda t). \end{aligned} \qquad (9)$$

Substitution of (9) into (7) and linearising about the travelling wave solution yields the eigenvalue problem:

$$\lambda\bar{u} = (2UW - b)\bar{u} + U^2\bar{w} + a^2(\bar{I} - \bar{u}) + c\bar{u}', \qquad (10a)$$

$$\lambda\bar{u} = -2UW\bar{u} - (1 + U^2)\bar{w} + a^2(\bar{I} - \bar{u})$$
$$+ (c + v)\bar{u}' + d\bar{u}'', \qquad (10b)$$

$$0 = a^2(\bar{u} - \bar{I}) + \bar{I}'' \qquad (10c)$$

Here, λ and the associated eigenvectors $\bar{u}$, $\bar{w}$, $\bar{I}$ are complex valued. The values of λ that satisfy (10) determine
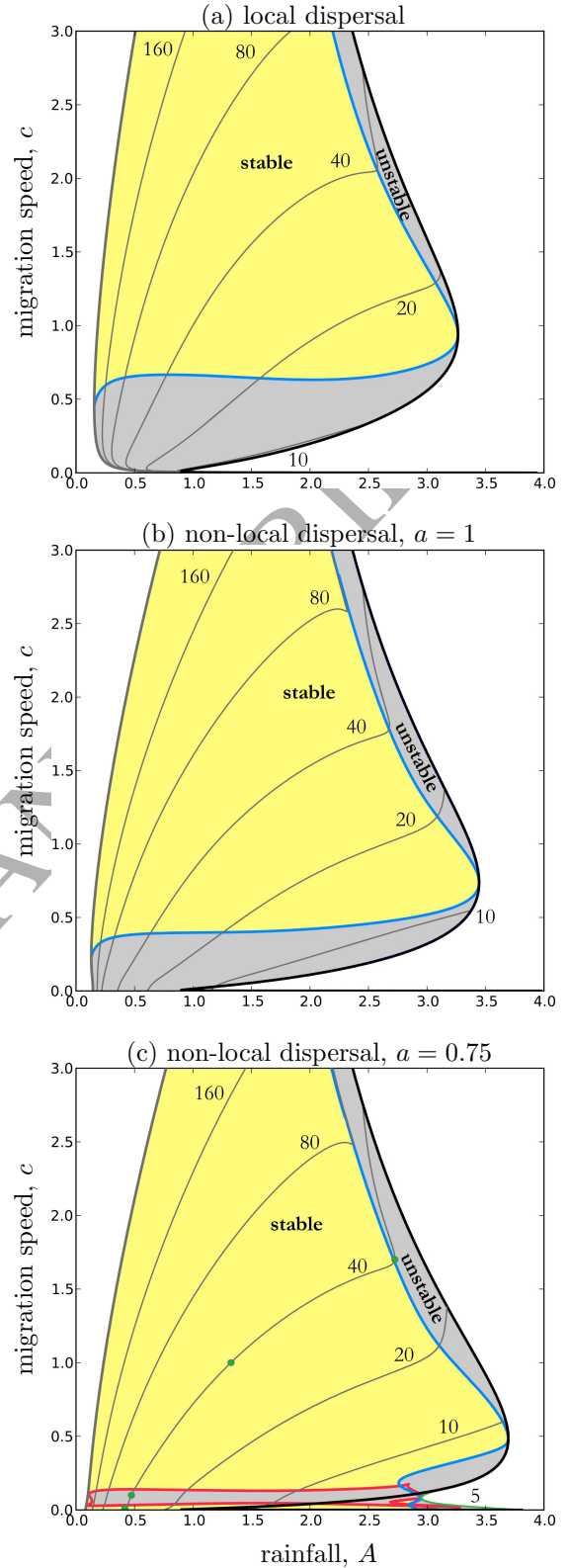

Figure 3: Existence and stability of striped vegetation patterns for (a) the local Klausmeier model, (b), (c) the non-local Klausmeier model with Laplace kernel and $C = a^2$. Thick black curve: Turing-Hopf locus. Thick grey curve: locus of homoclinic solutions. Thin grey curves: contours of constant wavelength. Blue curve: Eckhaus instability boundary. Red curve: Hopf instability boundary. Green curve: locus of folds. Yellow/grey regions indicate stable/unstable solutions. Green points represent solutions in Figure 2. Other model parameters are fixed: $B = 0.45$, $v = 182.5$, $d = 1$.
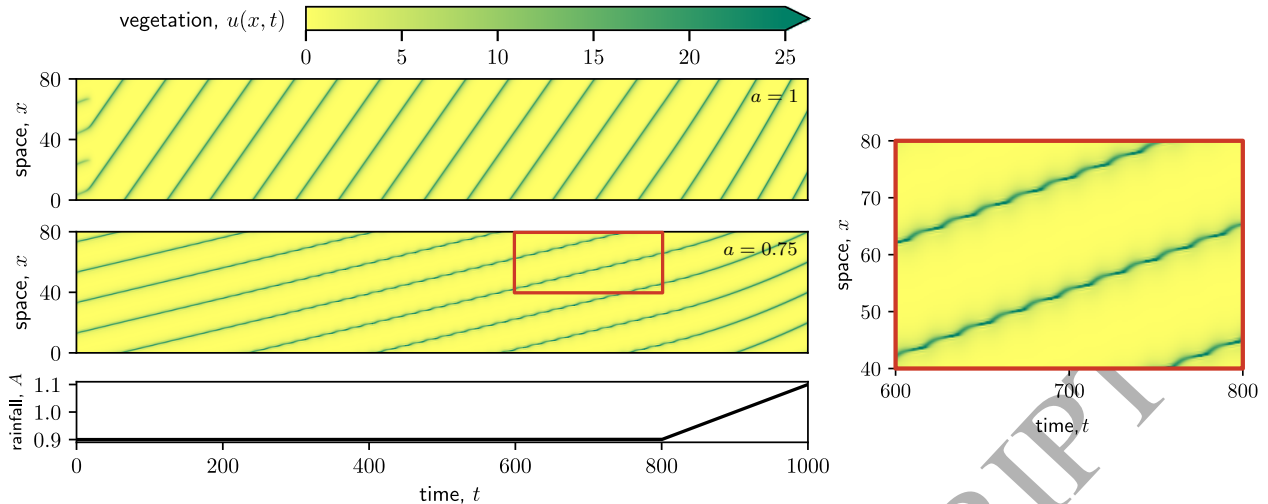
Figure 4: Resilience of patterns in the non-local Klausmeier model. The figure shows time simulations of two initially unstable patterns for different a. When $a = 1$ the initial pattern of wavelength 20 quickly destabilises to form a pattern of wavelength 40; this is because of an Eckhaus instability. When $a = 0.75$ temporal oscillations due to a Hopf instability are visible but the wavelength of the pattern remains the same and a small increase in rainfall regenerates a stable pattern with the same initial wavelength. Other model parameters are fixed: $B = 0.45$, $v = 182.5$, $d = 1$.

whether small disturbances will grow or decay, and is known as the spectrum. It is common practice to visualise spectra in the complex plane as we do in Figure 2 for different travelling wave solutions of (8). We use the method of Rademacher to plot the spectra associated with (10)—for details we refer the reader to [36, 43]. Note that the method involves discretising the eigenvalue problem in order to find approximate initial values of λ from which a numerical continuation can be started. For this, a minor complication is that (10) is a 'generalised' eigenvalue problem since (8c) has no time derivative. This is easily dealt with using a simple reformulation to the 'ordinary' case [43].

All spectra of travelling waves go through the origin in the complex λ plane (reflecting the neutral stability of the wave to translation) and so we must omit $\lambda = 0$ in the following definition of stability: if $\text{Re}(\lambda) < 0$ for all $\lambda \neq 0$ the solution is linearly stable; if there exists a λ with $\text{Re}(\lambda) > 0$ the solution is unstable. Figures 2(b,c) show stable solutions of 7, whereas Figures 2(a,c) show unstable solutions. The transition in Figures 2(a-d) is obtained by decreasing A; this affects the shape and stability of solutions. Consider the solution in Figure 2(b). Increasing the rainfall will eventually result in the solution in Figure 2(a) which is unstable as a result of an 'Eckhaus' (or 'sideband') instability—a change of curvature at the origin of the spectrum. This is a standard and well documented feature of the Klausmeier model and is the key to explaining the transition of vegetation patterns. A banded pattern that becomes unstable via Eckhaus instability switches to a pattern of longer/shorter wavelength. Decreasing the rainfall eventually gives the solution in Figure 2(c) which is unstable due to a 'Hopf' type instability. This has interesting implications on the future of an un-

stable pattern—for instance, instead of a transition to a different wavelength pattern as with an Eckhaus instability, the wavelength is preserved and temporal oscillations can be observed [44]. We address the ecological significance of this in the following section.

Using the ideas described so far we are able to map out existence and stability boundaries for banded vegetation patterns in the A–c parameter plane in Figure 3. We calculate stability boundaries via continuation of marginally stable solutions in parameter space. For an Eckhaus instability boundary, this involves finding a solution with zero curvature at $\lambda = 0$ in the spectrum. In contrast, a Hopf instability boundary is calculated via continuation of solutions with a double root for $\text{Re}(\lambda) = 0$ away from the origin.

2.3. Results

We have discussed the methods employed in this section for determining the existence and stability of solutions. We now examine the ecological implications of Figure 3. Results for the local Klausmeier model in Figure 3(a) are not novel, but we include them so a comparison may be made with results for the non-local Klausmeier model in Figure 3(b) and (c). As mentioned, when $C = a^2$ the non-local model approaches the local in the large a limit. We have repeated our numerical analysis for large a and obtain results indistinguishable from Figure 3(a), validating the predicted convergent behaviour.

In Figure 3(b,c) we map out pattern existence and stability in the A–c parameter plane for moderate values of a. Previous work [28] has focused only on the existence of patterns, concluding that the tendency for pattern formation increases as a decreases (with $C = a^2$). The Turing-Hopf bifurcation locus, from which patterns of constant

7

wavelength emanate, bounds the right-hand side of the pattern forming region; with a locus of homoclinic orbits bounding the left. Patterns can either be stable or unstable and we divide the pattern forming region accordingly.

305 Suppose one has a stable pattern; as one varies A the pattern evolves following a contour of constant wavelength (see Figure 1 for an illustration of this in a numerical simulation of the model). The pattern can become unstable as a result of either an increase, or a decrease in rainfall.

310 In this paper, we refer to a pattern becoming unstable due to increased rainfall as a 'transition towards uniform vegetation', and decreased rainfall as a 'transition towards desert'. Our numerical analysis in Figure 3 shows that the parameter region for stable patterns grows as a decreases.

315 Additionally, one can see that a transition towards desert occurs at lower rainfall levels along the wavelength contours. Interestingly, a transition towards uniform vegetation remains largely unchanged relative to the Turing-Hopf bifurcation locus. This reflects the increased resilience of

320 patterns at low rainfall when a is small, and a preference of the system to transition towards uniform vegetation as soon as the rainfall is sufficient to permit it.

For very long range dispersal (still with $C = a^2$), the mechanism of destabilisation can change completely from

325 an Eckhaus instability to a Hopf instability, though only in the region relevant to a transition towards desert. The ecological implications of this can be observed in numerical simulation of (4). Figure 4 shows time simulations of two initially unstable striped patterns for different a and

330 otherwise identical parameter values. The first is unstable because of an Eckhaus instability and quickly transitions to a longer wavelength pattern corresponding to a
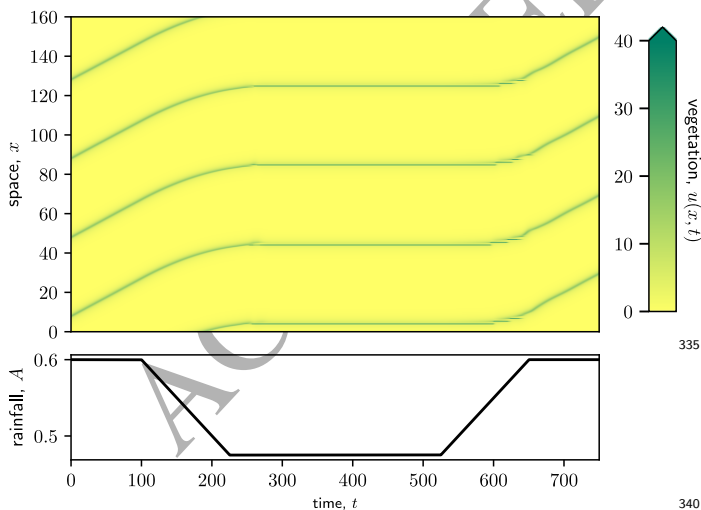

Figure 5: Stationary patterns in the non-local Klausmeier model. Initially we have a stable pattern. As the rainfall is reduced the pattern becomes unstable due to a Hopf type instability. This causes the pattern to halt its migration up the slope and stationary, high density peaks are observed. As rainfall increases back to its initial value, the initial stable pattern returns, highlighting the increased resilience of the system. This simulation was done with $a = 0.75$ and $d = 100$.
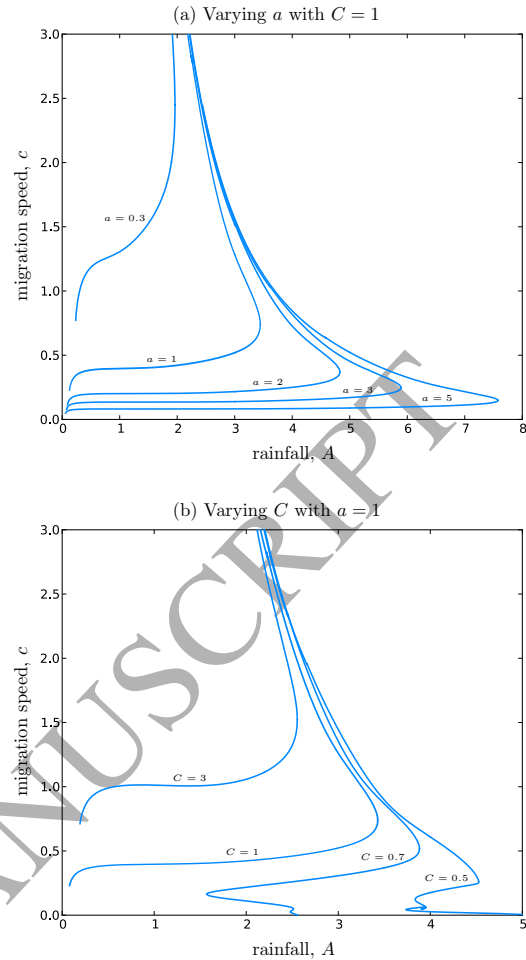

Figure 6: The variation in the Eckhaus stability boundary for (a) varying kernel width with fixed dispersal rate; (b) varying dispersal rate with fixed kernel width. The range of stable striped patterns grows as the Eckhaus boundary moves to the right. In (a) the Eckhaus boundary recedes to the left as the width of the kernel increases. In (b) the Eckhaus boundary grows to the right as the seed dispersal rate increases. All curves terminate at a point on the locus of homoclinic orbits (not shown) to the left of the plot, except for the curves in (b) with $C = 0.7$ and $C = 0.5$ which turn around and move towards the right. Here, a Hopf instability (not shown) becomes the primary destabilisation mechanism similarly to that shown in Figure 3(c). Other model parameters are fixed: $B = 0.45$, $v = 182.5$, $d = 1$.

shift towards the desert state. This behaviour is a key component of the original Klausmeier model and is well
335 established in the literature. The second is unstable because of a Hopf-type instability and as time evolves, the peaks of vegetation begin to oscillate in time. The wavelength of the pattern is preserved and a modest increase in rainfall allows a stable pattern to emerge. Intuitively, this
340 seems a valid ecological strategy: if the amount of rainfall cannot sustain the pattern, peaks of vegetation alternate their density to compensate for the lack of water in the overarching ecosystem. This ensures its structure is not lost so that when rainfall is increased, a stable pattern of the same (shorter) wavelength may persist.

In Figure 5 we show a similar time simulation of a pattern becoming unstable, again due to a Hopf type instabil-

ity, though with slightly different parameters. In this case we have an initially stable pattern that migrates uphill at a constant speed. As the rainfall is reduced the pattern begins to slow as expected close to destabilisation, and becomes unstable at approximately $A = 0.5$. This results in high density, stationary peaks of vegetation that remain at the same wavelength as the initial stable pattern. This is an unusual prediction for a model with directed transport. The most important feature for both of these observations—oscillating peaks and stationary patterns—is the ability of the ecosystem to endure the same arid conditions that would normally lead to catastrophe, according to the local Klausmeier model.

Finally in this section we comment that we are not aware of any ecological evidence for choosing $C = a^2 = 2/\sigma(a)^2$—we did so simply because of the associated convergence properties of (4) in the large a limit that allow for model comparison. Therefore, for completeness we performed our calculations for varying a with a fixed value of C, and vice versa. The Eckhaus stability boundary is particularly informative because it not only bounds the right hand side of the stable pattern forming region, but it must necessarily pass through the maximum A supporting pattern formation, and so for brevity we compare Eckhaus curves for various combinations of a and C in Figure 6. We discuss the separate cases: for fixed C, increasing the width of the dispersal kernel limits the range of stable patterns, with uniform vegetation being sustainable at much lower levels of rainfall. When patterned vegetation is observed for small a it is likely to have a faster migration speed, in contrast to large a values; for which vegetation is likely to have a low migration speed. For a fixed kernel width, a decreased dispersal rate will yield greater pattern forming tendencies, and in some cases the Eckhaus boundary may be replaced by a stability boundary of Hopf-type, changing the behaviour of unstable solutions as previously discussed. A comprehensive statistical assessment [31] of various ecological datasets suggests a range of C and a combinations that may occur for different plant species and dispersal modes. Although the relationship $C = a^2$ cannot in general be assumed, the parameter choices in Figure 3(c) along with subsequent conclusions are still relevant.

3. A comparison of kernels

3.1. Methods

The analysis of the non-local Klausmeier model for general seed dispersal kernels is very difficult and we are not aware of any methods that allow the insight and accuracy gained in Section 2, though efficient numerical simulations of integro-differential equation models are still possible (when the non-local term is a convolution) via use of fast Fourier transforms (FFTs)—see, for instance, [45, 46]. One approach used in the past has been to discretise the system in space in order to obtain a large system of ordinary differential equations [47]. The immediate drawback

of this is the increased computational expense of any numerical analysis, and in particular, testing the stability along solution branches is time consuming. The computation is, however, feasible on a coarse spatial grid at the expense of numerical accuracy. Therefore, the results in this section are qualitative and are intended for the purposes of comparison. In 2007, the local Klausmeier model was analysed in the same way [47], with the computation being implemented with a grid spacing of $\Delta x = 2$. With an increase in computational power since then, we are able to use $\Delta x = 1$, and with a more complicated set of equations. As technology advances it will become possible to employ this method with a finer grid spacing to obtain more accurate results.

The spatial discretisation of the non-local Klausmeier model gives the following system of ODEs:

$$\frac{\partial u_i}{\partial t} = u_i^2 w_i - B u_i + C(I_i - u_i), \tag{11a}$$

$$\frac{\partial w_i}{\partial t} = A - w_i - u_i^2 w_i + v \frac{w_{i+1} - w_i}{\Delta x} + d \frac{w_{i+1} - 2w_i + 2w_{i-1}}{\Delta x^2} \tag{11b}$$

for $i = (1, ..., N)$ and where I_i is an approximation of the infinite integral. We consider periodic boundary conditions $u_0(t) = u_N(t)$, $u_{N+1}(t) = u_1(t)$, $w_0(t) = w_N(t)$, $w_{N+1}(t) = w_1(t)$ for simplicity. If one truncates the integral to be evaluated on the interval $[-L, L]$, we can work on the same grid as (11) and define M points for the integral approximation as $y_j = -L + (j-1)\Delta x$ with $j = (1, ..., M)$ and $M = 2L/\Delta x + 1$. The set of points y_j is then a subset of x_i and we can use, for example, the trapezoidal rule to obtain the following approximation:

$$I_i(t) = \frac{\Delta x}{2} \sum_{j=1}^{M} \left(\phi(y_{j-1}) u(x_i - y_{j-1}, t) + \phi(y_j) u(x_i - y_j, t) \right). \tag{12}$$

Some kernels we studied required Simpson's rule for a more accurate approximation. L must be carefully chosen—not too large so as to needlessly increase computational cost, and not too small so that one obtains a poor approximation of the infinite integral. For instance, if the width of the kernel in question is small in comparison with the length of the spatial domain, one can take M to be significantly less than N, reducing the computation time.

Our approach to balance accuracy and efficiency was as follows: we chose a dispersal kernel and calculated an accurate 'true' evaluation of $\int_{-L}^{L} \phi(x) dx$ to verify that the truncation is sufficiently close to 1, keeping L as small as possible. We then calculated the numerical approximation on our coarse grid spacing and compared it with the true result. Clearly one can choose a kernel which is not well approximated with such a course grid spacing, though the kernels and parameters we used were 'nice' enough for this method. Assuming a well approximated kernel is obtained,
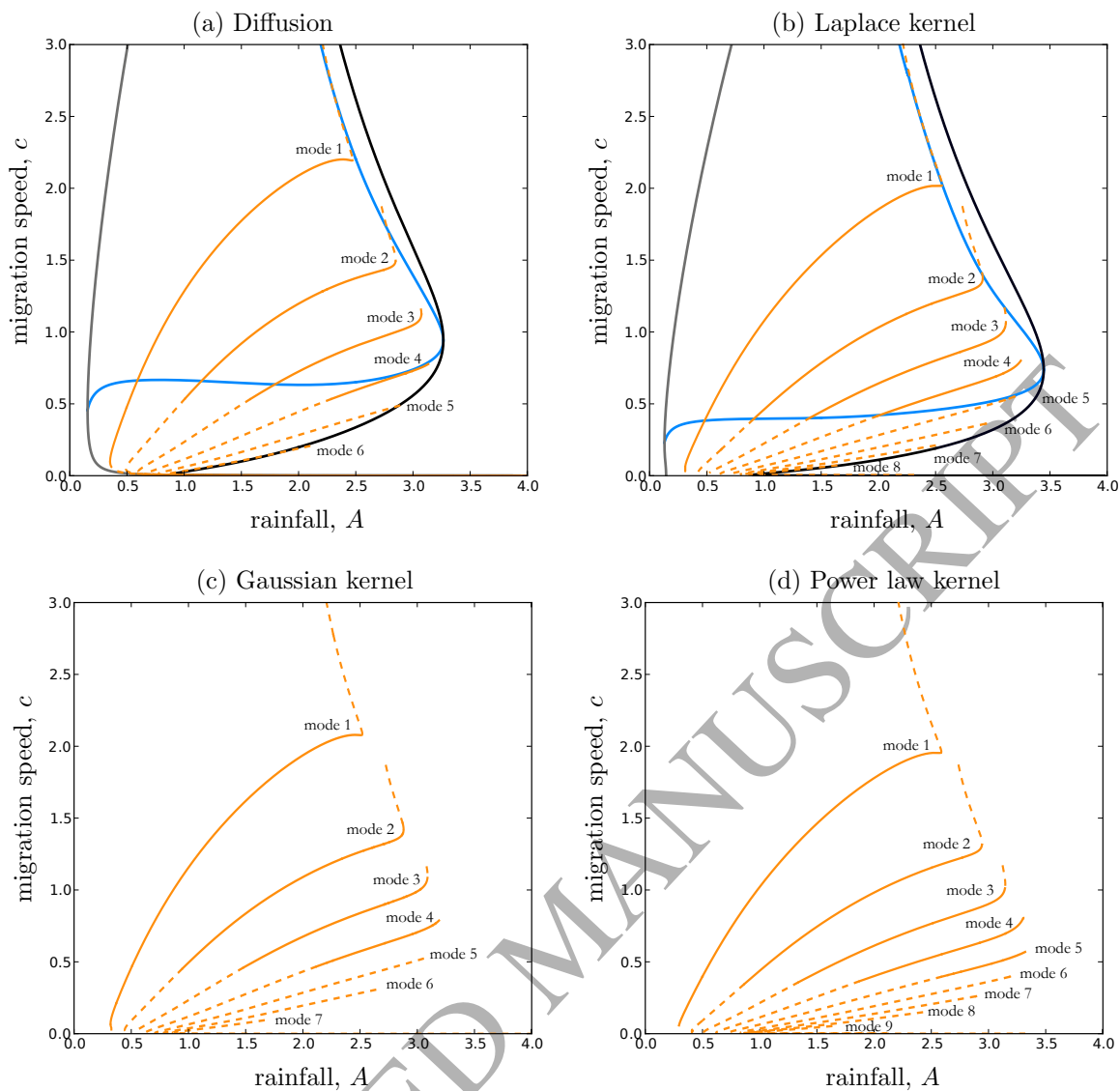
Figure 7: Existence and stability results for various dispersal kernels using (11) are plotted in orange with solid/dashed curves representing stable/unstable solutions. Known results for the Hopf locus (black) and Eckhaus stability boundary (blue) obtained using the methods in Section 2.2 are superimposed in (a) and (b). The standard deviation and dispersal rates in (b)-(d) were kept constant: $\sigma^2 = 2$, $C = 1$. Other model parameters are fixed: $B = 0.45$, $v = 182.5$, $d = 1$.

one can begin the analysis of (11) which we do, again, by numerical continuation with AUTO 07p [42].

Our analysis begins with the stable homogeneous steady state of uniform vegetation. For the spatially discretised system of equations, as one decreases the rainfall parameter the homogeneous steady state becomes unstable, and one detects a number of Hopf bifurcations corresponding to a selection of specific pattern modes which depend on the size of the spatial domain—in this paper we take the domain size to be 60, and with a grid spacing of $\Delta x = 1$ this gives us 120 equations to analyse. One then numerically continues periodic solutions from each detected Hopf bifurcation allowing AUTO to test stability as the rainfall parameter varies along the solution branch.

We study (4) for three ecologically relevant kernels, along with the diffusion case (1), for which this analysis

was applied for $d = 0$ in [47]. Together with the Laplace kernel (6) we consider a Gaussian kernel

$$\phi(x) = \frac{a_g}{\sqrt{\pi}} e^{-a_g^2 x^2}, \quad a_g > 0, \tag{13}$$

and a power law kernel

$$\phi(x) = \frac{(b-1)a_p}{2(1 + a_p|x|)^b}, \quad a_p > 0, \ b > 3. \tag{14}$$

The standard deviations for the Laplace, Gaussian and power law kernels are $\sigma(a) = \sqrt{2}/a$, $\sigma(a_g) = 1/(\sqrt{2}a_g)$ and $\sigma(a_p) = (\sqrt{b^2 - 5b + 6a_p})$, respectively. Since the power law kernel is a two-parameter kernel we fixed $b = 10$. For comparison we take $C = 1$ and choose kernel parameters such that $\sigma = \sqrt{2}$ in each case, so that $a = 1$, $a_g = 0.5$ and $a_p \approx 0.134$. AUTO will not distinguish between an

Eckhaus or a Hopf type instability so we choose C not too small so as not to generate a Hopf-type instability (see Figure 6(b)). To be clear, we are now comparing between the shape of the kernel, as opposed to its width as in Section 2.

3.2. Results

The functional form of the dispersal kernel has a minimal influence on the formation and evolution of striped patterns as seen in Figure 7, and more significant differences are observed when one varies the width of the kernel and the rate of dispersal. Consequently, the conclusions set out in Section 2 become more important; now being relevant to a wider variety of plant species that disperse seeds according to a range of dispersal kernels. We do however discuss the small variations that occur when one changes ϕ.

We overlay the known results for diffusion and Laplace kernel cases in Figure 7(a,b), allowing one to gauge the accuracy of the discussed spatial approximation. We retain surprising levels of accuracy despite the coarseness of the spatial grid, especially when ϕ is the Laplace kernel. Note that the maximum rainfall for pattern formation (the intersection of Eckhaus and Hopf-locus curves) is only relevant for periodic boundary conditions when the domain size is divisible by the pattern wavelength—a quasi-periodic solution would be unstable as a solution of the underlying model and patterns would not be observed. Qualitatively, the existence and stability of patterns is the same regardless of the shape of the dispersal kernel, assuming a fixed kernel width. The main difference is the existence of additional pattern modes when one considers non-local dispersal as opposed to local dispersal, though these are mostly unstable and therefore irrelevant in applications. There is also a difference in this respect when one changes the shape of the kernel, with the least pattern modes being observed for a Gaussian kernel, and the most for a power law kernel.

Because the differences are slight, it is more convenient to view the threshold existence and stability values as a function of the pattern wavelength, as we show in Figure 8 for the relevant stable patterns only. We find that the power law and Laplace kernels in particular increase the pattern forming tendencies as well as resilience. For the Laplace, Gaussian and diffusion cases the onset of pattern formation generates a mode 4 pattern but for the power law kernel, a mode 5 pattern becomes relevant at onset. In ecological terms, plants that disperse their seeds according to a power law distribution are more likely to form shorter wavelength patterns with increased resilience. The unfortunate downside of the increased resilience observed in the Laplace and power law cases is the additional rainfall needed for ecosystem restoration. For instance, consider the mode 1 pattern corresponding to an oasis on the periodic domain of length 60. It is true that the Laplace and power law distributions allow the pattern to persist at lower rainfall levels than the Gaussian and diffusion cases.
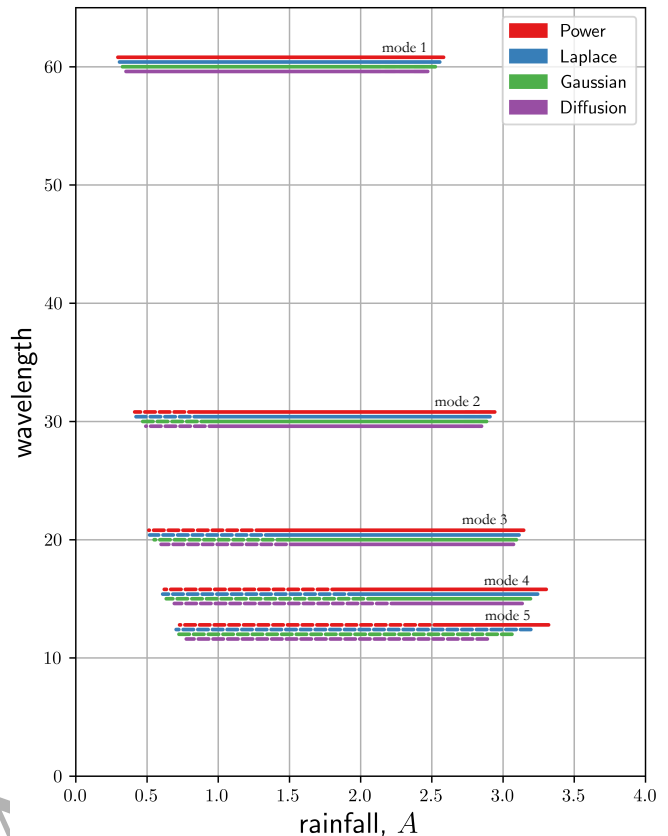

Figure 8: A comparison of the relevant stable patterns according to their wavelength for a range of dispersal kernels. Parameters are $C = 1$, $\sigma^2 = 2$ with other model parameters given in the main body of the text. Solid/dashed lines represent stable/unstable patterns. Other model parameters are fixed: $B = 0.45$, $v = 182.5$, $d = 1$.

However, upon increasing the rainfall the system is more easily restored in the Gaussian and diffusion cases meaning a trade off exists, with a price to pay for increased resilience.

4. Discussion

Striped patterns are strongly influenced by non-local seed dispersal. Our findings in Section 2 reveal that non-local dispersal can increase the resilience of striped vegetation in two ways: the first by permitting stable patterns at levels of rainfall that would otherwise be unsustainable if seeds dispersed locally. The second is more interesting; patterns undergo the usual slowing down when rainfall approaches critically low levels, but in certain instances patterns that become 'unsustainable' do not lead to a sudden shift of the ecosystem towards desert, as previous theory suggests. Instead the model predicts alternative coping strategies such as fluctuations of vegetation peak densities in time (see Figure 4) and even stationary patterns (see Figure 5). In both cases a small increase in rainfall regen-

erates the previous stable pattern, which demonstrates the increased resilience of the vegetation as a consequence of long-distance seed dispersal.

A key finding of our work is the existence of slow moving and stationary patterns as a result of non-local dispersal. There is much evidence to support the uphill migration of vegetation stripes, both mathematical [34] and empirical [48, 34]. However, contradictory field observations also exist that suggest patterns can be stationary on slopes [15, 49] with the local Klausmeier model being inconsistent with such evidence. Other theoretical models have been proposed that do permit stationary solutions [50, 51]—they include the transport of seeds via run-off water in the downhill direction. It has also been posited that stationary patterns could be explained by compacted, weathered bands of soil that make colonisation difficult [7]. The original Klausmeier model was deemed to be in order-of-magnitude agreement with field observations [26] and gave predictions of migration speeds in the range $0.4 - 1.9$ m year^{-1}. With the addition of non-local dispersal, patterns may be permitted at $c < 0.2$ in some cases (see Figure 6(a)) corresponding to speeds of < 0.1 m year^{-1}—the movement of vegetation would be practically undetectable over the time span of the available data. Although (4) is not intended to be quantitatively accurate, we believe the model provides a good explanation for why patterns may be observed as stationary in practice.

The motivation for studying the affects of dispersal kernel shape was the wide extent of factors affecting dispersal distance (e.g. vegetation species, habitat, dispersal mode). Certainly a single kernel cannot be fitted to every dataset across all plant species. In particular, a main feature of many ecologically relevant dispersal kernels are their 'fat' tails—these are often called 'leptokurtic' kernels. The power law kernel can be viewed as fat tailed due to its algebraic decay away from the mean, contrary to the exponential decay of the 'thin' tailed Gaussian and Laplace kernels. In general, however, we find that existence and stability are very similar regardless of kernel which suggests that kernel width and seed dispersal rate are more relevant in the study of patterned vegetation, and the kernel shape can be neglected for qualitative studies. This strengthens our results that assume Laplace distributed seed dispersal in Section 2.

A direction for further studies could be the (possible) existence of stable stationary patterns in the non-local Klausmeier model as suggested by Figure 3(c). For the local model the homoclinic orbit locus terminates at the Hopf bifurcation locus, though despite our efforts we were unable to determine whether this non-occurrence in Figures 3(b-c) was a numerical issue or a genuine feature of the model; wavelength contours do appear to terminate very close to a zero migration speed. One can observe similar behaviour for the spatially discretised system in Figure 7. We were unable to verify the behaviour in time simulations of the model due to the sharpness of the vegetation peaks which lead to a poor approximation in our

numerical scheme—a more sophisticated algorithm is required here, e.g. dynamically varying mesh. Furthermore, an interesting direction would be to try and estimate the kernel parameters and dispersal rate in a specific instance of banded vegetation as a case study. In particular, one could estimate the parameters for vegetation that has been shown to exhibit uphill migration, and vegetation shown to be stationary. Feeding these parameters into the model could help verify our theory as to why some patterns move, and some do not.

5. References

References

[1] W. Macfadyen, Vegetation patterns in the semi-desert plains of British Somaliland, The Geographical Journal 116 (4/6) (1950) 199–211.

[2] C. Valentin, J.-M. d'Herbès, J. Poesen, Soil and water components of banded vegetation patterns, Catena 37 (1-2) (1999) 1–24.

[3] J. Thiery, J.-M. d'Herbes, C. Valentin, A model simulating the genesis of banded vegetation patterns in Niger, Journal of Ecology (1995) 497–507.

[4] J. Müller, Floristic and structural pattern and current distribution of tiger bush vegetation in Burkina Faso (West Africa), assessed by means of belt transects and spatial analysis, Applied Ecology and Environmental Research 11 (2013) 153–171.

[5] D. J. Tongway, J. A. Ludwig, Vegetation and soil patterning in semi-arid Mulga Lands of eastern Australia, Austral Ecology 15 (1) (1990) 23–34.

[6] M. Moreno-de las Heras, P. M. Saco, G. R. Willgoose, D. J. Tongway, Variations in hydrological connectivity of Australian semiarid landscapes indicate abrupt changes in rainfall-use efficiency of vegetation, Journal of Geophysical Research, Biogeosciences 117 (G3).

[7] D. Dunkerley, K. Brown, Oblique vegetation banding in the Australian arid zone: implications for theories of pattern evolution and maintenance, Journal of Arid Environments 51 (2) (2002) 163–181.

[8] J. D. Pelletier, S. B. DeLong, C. A. Orem, P. Becerra, K. Compton, K. Gressett, J. Lyons-Baral, L. A. McGuire, J. L. Molaro, J. C. Spinler, How do vegetation bands form in dry lands? Insights from numerical modeling and field studies in southern Nevada, USA, Journal of Geophysical Research, Earth Surface 117 (F4).

[9] G. G. Penny, K. E. Daniels, S. E. Thompson, Local properties of patterned vegetation: quantifying endogenous and exogenous effects, Philosophical Transactions of the Royal Society of London, Series A: Mathematical, Physical and Engineering Sciences 371 (2004) (2013) 20120359.

[10] M. R. Aguiar, O. E. Sala, Patch structure, dynamics and implications for the functioning of arid ecosystems, Trends in Ecology & Evolution 14 (7) (1999) 273–277.

[11] J. von Hardenberg, E. Meron, M. Shachak, Y. Zarmi, Diversity of vegetation patterns and desertification, Physical Review Letters 87 (19) (2001) 198101.

[12] H. Yizhaq, S. Sela, T. Svoray, S. Assouline, G. Bel, Effects of heterogeneous soil-water diffusivity on vegetation pattern formation, Water Resources Research 50 (7) (2014) 5743–5758.

[13] S. Thompson, G. Katul, A. Konings, L. Ridolfi, Unsteady overland flow on flat surfaces induced by spatial permeability contrasts, Advances in Water Resources 34 (8) (2011) 1049–1058.

[14] C. Hemming, Vegetation arcs in Somaliland, Journal of Ecology (1965) 57–67.

[15] G. Worrall, The Butana grass patterns, European Journal of Soil Science 10 (1) (1959) 34–53.

[16] C. Montana, The colonization of bare areas in two-phase mosaics of an arid ecosystem, Journal of Ecology (1992) 315–327.

[17] N. Thomas, S. Nigam, Twentieth-century climate change over Africa: seasonal hydroclimate trends and Sahara Desert expansion, Journal of Climate 31 (9) (2018) 3349–3370.

[18] M. Rietkerk, S. C. Dekker, P. C. De Ruiter, J. van de Koppel, Self-organized patchiness and catastrophic shifts in ecosystems, Science 305 (5692) (2004) 1926–1929.

[19] S. Kéfi, M. Rietkerk, C. L. Alados, Y. Pueyo, V. P. Papanastasis, A. ElAich, P. C. De Ruiter, Spatial vegetation patterns and imminent desertification in Mediterranean arid ecosystems, Nature 449 (7159) (2007) 213.

[20] R. Corrado, A. M. Cherubini, C. Pennetta, Early warning signals of desertification transitions in semiarid ecosystems, Physical Review E 90 (6) (2014) 062705.

[21] S. Kéfi, V. Guttal, W. A. Brock, S. R. Carpenter, A. M. Ellison, V. N. Livina, D. A. Seekell, M. Scheffer, E. H. van Nes, V. Dakos, Early warning signals of ecological transitions: methods for spatial patterns, PLOS ONE 9 (3) (2014) e92097.

[22] J. A. Sherratt, When does colonisation of a semi-arid hillslope generate vegetation patterns?, Journal of Mathematical Biology 73 (1) (2016) 199–226.

[23] M. Rietkerk, M. C. Boerlijst, F. van Langevelde, R. HilleRisLambers, J. v. de Koppel, L. Kumar, H. H. Prins, A. M. de Roos, Self-organization of vegetation in arid ecosystems, The American Naturalist 160 (4) (2002) 524–530.

[24] E. Gilad, J. von Hardenberg, A. Provenzale, M. Shachak, E. Meron, Ecosystem engineers: from pattern formation to habitat creation, Physical Review Letters 93 (9) (2004) 098105.

[25] E. Gilad, J. von Hardenberg, A. Provenzale, M. Shachak, E. Meron, A mathematical model of plants as ecosystem engineers, Journal of Theoretical Biology 244 (4) (2007) 680–691.

[26] C. A. Klausmeier, Regular and irregular patterns in semiarid vegetation, Science 284 (5421) (1999) 1826–1828.

[27] S. A. Cannas, D. E. Marco, M. A. Montemurro, Long range dispersal and spatial pattern formation in biological invasions, Mathematical Biosciences 203 (2) (2006) 155–170.

[28] L. Eigentler, J. A. Sherratt, Analysis of a model for banded vegetation patterns in semi-arid environments with nonlocal dispersal, Journal of Mathematical Biology (2018) 1–25.

[29] Y. Pueyo, S. Kefi, C. Alados, M. Rietkerk, Dispersal strategies and spatial organization of vegetation in arid ecosystems, Oikos 117 (10) (2008) 1522–1532.

[30] M. de Jager, F. J. Weissing, P. M. Herman, B. A. Nolet, J. van de Koppel, Lévy walks evolve through interaction between movement and environmental complexity, Science 332 (6037) (2011) 1551–1553.

[31] J. M. Bullock, L. Mallada González, R. Tamme, L. Götzenberger, S. M. White, M. Pärtel, D. A. Hooftman, A synthesis of empirical plant dispersal kernels, Journal of Ecology 105 (1) (2017) 6–19.

[32] M. G. Neubert, M. Kot, M. A. Lewis, Dispersal and pattern formation in a discrete-time predator-prey model, Theoretical Population Biology 48 (1) (1995) 7–43.

[33] H. G. Othmer, S. R. Dunbar, W. Alt, Models of dispersal in biological systems, Journal of Mathematical Biology 26 (3) (1988) 263–298.

[34] J. A. Sherratt, Pattern solutions of the Klausmeier model for banded vegetation in semiarid environments IV: Slowly moving patterns and their stability, SIAM Journal on Applied Mathematics 73 (1) (2013) 330–350.

[35] J. A. Sherratt, Pattern solutions of the Klausmeier model for banded vegetation in semiarid environments V: the transition from patterns to desert, SIAM Journal on Applied Mathematics 73 (4) (2013) 1347–1367.

[36] J. Rademacher, B. Sandstede, A. Scheel, Computing absolute and essential spectra using continuation, Physica D: Nonlinear Phenomena 229 (2007) 166–183.

[37] J. Clobert, Dispersal ecology and evolution, Oxford University Press, 2012.

[38] C. R. Laing, W. C. Troy, B. Gutkin, G. B. Ermentrout, Multiple bumps in a neuronal model of working memory, SIAM Journal on Applied Mathematics 63 (1) (2002) 62–97.

[39] D. Avitabile, H. Schmidt, Snakes and ladders in an inhomogeneous neural field model, Physica D: Nonlinear Phenomena 294 (2015) 24–36.

[40] S. M. Merchant, W. Nagata, Selection and stability of wave trains behind predator invasions in a model with non-local prey competition, IMA Journal of Applied Mathematics 80 (2015) 1155–1177.

[41] J. A. Sherratt, Invasion generates periodic traveling waves (wavetrains) in predator-prey models with nonlocal dispersal, SIAM Journal on Applied Mathematics 76 (2016) 293–313.

[42] E. J. Doedel, T. F. Fairgrieve, B. Sandstede, A. R. Champneys, Y. A. Kuznetsov, X. Wang, Auto-07p: Continuation and bifurcation software for ordinary differential equations, Tech. rep. (2007).

[43] J. A. Sherratt, Numerical continuation methods for studying periodic travelling wave (wavetrain) solutions of partial differential equations, Applied Mathematics and Computation 218 (9) (2012) 4684–4694.

[44] A. S. Dagbovie, J. A. Sherratt, Pattern selection and hysteresis in the Rietkerk model for banded vegetation in semi-arid environments, Journal of the Royal Society, Interface 11 (99) (2014) 20140465.

[45] S. Coombes, H. Schmidt, I. Bojak, Interface dynamics in planar neural field models, Journal of Mathematical Neuroscience 2 (1) (2012) 9.

[46] J. Rankin, D. Avitabile, J. Baladron, G. Faye, D. J. Lloyd, Continuation of localized coherent structures in nonlocal neural field equations, SIAM Journal on Scientific Computing 36 (1) (2014) B70–B93.

[47] J. A. Sherratt, G. J. Lord, Nonlinear dynamics and pattern bifurcations in a model for vegetation stripes in semi-arid environments, Theoretical Population Biology 71 (1) (2007) 1–11.

[48] V. Deblauwe, P. Couteron, J. Bogaert, N. Barbier, Determinants and dynamics of banded vegetation pattern migration in arid climates, Ecological Monographs 82 (1) (2012) 3–21.

[49] L. White, Vegetation arcs in Jordan, Journal of Ecology (1969) 461–464.

[50] P. Saco, G. Willgoose, G. Hancock, Eco-geomorphology of banded vegetation patterns in arid and semi-arid regions, Hydrology and Earth System Sciences Discussions 11 (6) (2007) 1717–1730.

[51] S. Thompson, G. Katul, Secondary seed dispersal and its role in landscape organization, Geophysical Research Letters 36 (2).